Original

Soininen, A.J.; Appavou, M.-S.; Frykstrand, S.; Welch, K.; Khaneft, M.;
Kriele, A.; Bellissent-Funel, M.-C.; Stroemme, M.; Wuttke, J.:

Dynamics of water confined in mesoporous magnesium carbonate

In: The Journal of Chemical Physics (2019) AIP

DOI: 10.1063/1.4971285

Dynamics of water confined in mesoporous magnesium carbonate

Antti J. Soininen,[1,2,a] Marie-Sousai Appavou,[1] Sara Frykstrand,[3] Ken Welch,[3] Marina Khaneft,[1] Armin Kriele,[4] Marie-Claire Bellissent-Funel,[5] Maria Strømme,[3] and Joachim Wuttke[1]

[1]*Jülich Centre for Neutron Science at MLZ, Forschungszentrum Jülich GmbH, Lichtenbergstraße 1, 85747 Garching, Germany*
[2]*Institut Laue-Langevin, 71 Avenue des Martyrs, 38042 Grenoble, France*
[3]*Division for Nanotechnology and Functional Materials, Department of Engineering Sciences, The Ångström Laboratory, Uppsala University, P.O. Box 534, 75121 Uppsala, Sweden*
[4]*German Engineering Materials Science Centre (GEMS) at MLZ, Helmholtz-Zentrum Geesthacht GmbH, Lichtenbergstrasse 1, 85747 Garching, Germany*
[5]*Laboratoire Léon Brillouin, CEA, CNRS, Université Paris-Saclay, CEA Saclay, 91191 Gif-sur-Yvette, France*

(Received 25 June 2016; accepted 14 November 2016; published online 15 December 2016)

We have measured the dynamics of water confined in a porous magnesium carbonate material, Upsalite®, using the high-resolution neutron backscattering spectrometer SPHERES. We found quasielastic scattering that does not flatten out up to 360 K, which means that the dynamics of water are much slower than in other matrix materials. Specifically, a single Lorentzian line could be fitted to the quasielastic part of the acquired spectra between 220 and 360 K. This, accompanied by an elastic line from dynamically frozen water present at all experimental temperatures, even above the melting point, signaled a significant amount of bound or slow water. *Published by AIP Publishing.* [http://dx.doi.org/10.1063/1.4971285]

I. INTRODUCTION

Water confined in pockets of a few nanometers in size can be found in numerous systems, ranging from porous minerals to biological environments. Confined water is quite different from bulk water as interfacial effects and geometrical constraints strongly alter its structure and dynamics. The changes depend on the chemistry of the confining interfaces and on the size and topology of the confining volume. To understand the convoluted interplay of these interactions, the behavior of confined water needs to be studied in a wide range of different environments.

Generally, confinement slows down the dynamics of water molecules and distorts the hydrogen bond network compared to liquid bulk water. Geometrical effects, such as reduced dimensionality, finite size effects, and curvature, hinder the ability of the water molecules to form their usual tetrahedrally bonded network and restrict long-range displacements.[1,2] In extreme confinements, like in carbon nanotubes, altogether new structures may arise.[3,4] Additionally, interactions with hydrophilic cavity walls reorient the water molecules near the surface, further affecting the hydrogen bond network.[2,5–7] Anchoring of water at the surface by hydrophilic interactions and surface roughness creates a dynamical gradient in the confining volume as water bound to the walls has slower translational dynamics compared to non-bound water in the center of the cavity.[2,7–9] Hydrophobic interfaces, on the other hand, have only weak interactions with water molecules and thus a weaker effect on the structure or dynamics.[10–12]

Upsalite® is a novel magnesium carbonate material with amorphous pore network which can be synthesized without the use of the surfactant templates needed for many other porous materials.[13] While Upsalite could find usage as a drug solubility enhancing agent,[14,15] and in other life science applications,[16,17] it was its intriguing hydration properties[13] which prompted us to study the dynamics of water inside its pores, using quasi-elastic neutron scattering (QENS).

Compared to the usual model systems, such as Vycor glass[1,18–21] or MCM-41 silica,[8,22–29] Upsalite is a more complex case to study. It has, for example, bimodal pore size distribution whereas MCM-41 has its pores in a well-defined hexagonal pattern. As the freezing point of water depends on the size of the confining volume,[2,30,31] we could identify two separate freezing points in Upsalite using differential scanning calorimetry (DSC).

The freezing point depression in porous materials also enables one to study the confined water dynamics at supercooled temperatures. The high-resolution neutron spectrometers typically employed for this cannot usually trace the dynamics much beyond the melting point within their energy window. Surprisingly, we found this not to be the case with Upsalite in which we could quantify the dynamics close to the boiling point of water. Thus, here we report for the first time QENS results on water confined in Upsalite up to temperatures and only a few studies on confinement have reached previously.[32–34]

II. EXPERIMENTAL

A. Sample preparation for QENS

Upsalite can be synthesized at low temperatures without using surfactant templates.[13] In short, a mixture of methanol

[a]Electronic mail: soininen@ill.fr

and MgO is stirred under 3 bars carbon dioxide atmosphere at 50 °C for 2.5 h. Subsequently, heating is turned off and the pressure is lowered to 1 bar. After the solution becomes light yellow in color, the carbon dioxide atmosphere is removed and a gel develops in the reaction vessel. Upon heating the gel to 70 °C, it solidifies forming the final porous $MgCO_3$/MgO powder. The surface of newly synthesized Upsalite is covered by organic residues which can be removed by calcination at temperatures above 250 °C.[35] Calcinated Upsalite has a bimodal distribution of pore sizes.[35] The major mode has a diameter around 55 Å while the diameters of the distinct minor mode fall below 20 Å. The relative volume of the smaller pores is almost negligible, and consequently, most water is expected to be found in the larger pores.

Two samples of calcinated Upsalite from different synthesis batches were hydrated for the neutron experiments (see supplementary material for details). One reached the hydration level of 0.367 g of water per 1 g of Upsalite (hereafter called U1) and another 0.463 g/g of water (U2). Additionally, a DRY sample from the same batch as U2 was prepared to serve as a reference. The total pore volume of the calcinated Upsalite was 0.42 cm^3/g according to N_2 adsorption experiments.[35] Thus, U2 can be regarded as fully hydrated whereas U1 may contain incompletely filled pores. The neutron transmission of the hydrated samples is estimated to be around 0.85.

MCM-41 with a hydration level of 0.45 g/g was used as an additional reference sample (see supplementary material for details). The material was synthesized from silica gel using ammonium surfactant $C_{10}H_{21}$-$(CH_3)_3N^+$ as a template resulting in pores with 21 Å in diameter.[36]

B. Sample characterization with DSC and X-ray diffraction (XRD)

For the interpretation of QENS data, it is important to know the state of hydration water during the experiment. Differential scanning calorimetry (DSC) measurements were therefore performed to study the extend of freezing at supercooled temperatures. Another concern is whether the matrix material was inert after the neutron experiments. Calcinated Upsalite is known to start to slowly crystallize after a week's exposure to water.[35] The possible presence of this crystalline phase was studied post-experiment by X-ray diffraction (XRD).

For DSC (Perking Elmer DSC 8500, nitrogen purged) we used Upsalite from the same synthesis batch from which the neutron sample U2 was made. Samples with different hydration levels were produced and encapsulated immediately in aluminium pans to avoid water evaporation. DSC scans between 298 and 178 K were performed with different cooling and heating rates. By repeating one cooling and heating cycle with identical rates, it was found that the heat flow curves are perfectly reproducible.

The heat flow curve of a sample with 0.426 g/g of water for cooling in Fig. 1 shows two exothermic freezing peaks f and f′ in contrast to bulk water which shows only a single sharp liquid-solid phase transition f_{water}. As a rule, the smaller the pore diameter, the lower is the freezing point.[30,37] Therefore it might be that the two DSC peaks reflect the bimodal

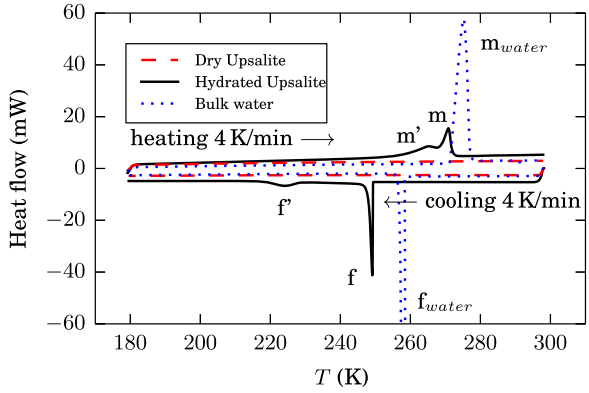

FIG. 1. DSC on dry non-calcinated Upsalite (red dashed line), with 0.426 g/g hydration (black solid line), and bulk water (blue dotted line) at 4 K/min heating/cooling rate.

pore size distribution in Upsalite. On the other hand, additional freezing peaks also appear at partially filled pores or at phase transitions of water films at the pore walls for all pore filling levels.[37] Both freezing peaks f and f′ are shifted to lower temperatures compared to the bulk water which indicates the presence of supercooled water. The onset temperatures of the freezing peaks are 280 K for bulk water and 257 K for f and 249 K for f′ of Upsalite with 0.426 g/g. Note, however, that the released heat (the area under the peaks) is no measure for the relative amount of freezable water in the wide and narrow pores: the enthalpy of freezing is temperature dependent and also varies with pore diameter.[31,38] From the studies of other porous materials, e.g., Vycor, it is well known that the presence of a frozen water fraction does not preclude relaxation dynamics in the unfreezable interface water to persist down to temperatures far below any freezing point.[39]

The QENS experiment lasted a total of seven (U1) or eight (U2) days, including sample preparation. To check if crystallization had occurred in the matrix material during the experiment, U2 and DRY were redried immediately after the scattering experiment and studied with XRD using Cu K_α radiation (wavelength 1.54 Å). As Fig. 2 shows, diffraction peaks characteristic of hydromagnesite ($Mg_5(CO_3)4(OH)_2 \cdot 4H_2O$) and nesquehonite ($MgCO_3 \cdot 3H_2O$) were found in U2, but were absent in DRY. So crystallization had indeed occurred in U2, and part of the adsorbed water had become chemically bound, mostly as water of crystallization. Our neutron scattering data, discussed below, indicate that this chemical reaction had only taken place near the end of the experiment, when the temperature was 340 K and above.

C. QENS experiments

Quasielastic neutron scattering was measured in November 2013 (MCM-41), February 2014 (U1), and May 2015 (U2, DRY) using the backscattering spectrometer SPHERES[40,41] at Heinz Maier-Leibnitz Zentrum in Garching, Germany. The experiments were conducted in transmission geometry with the sample cells oriented at 45° to the neutron beam. U1 was measured for 3 h at 3 K and for 6 h at nine temperatures between 180 and 290 K. Based on prior experience on

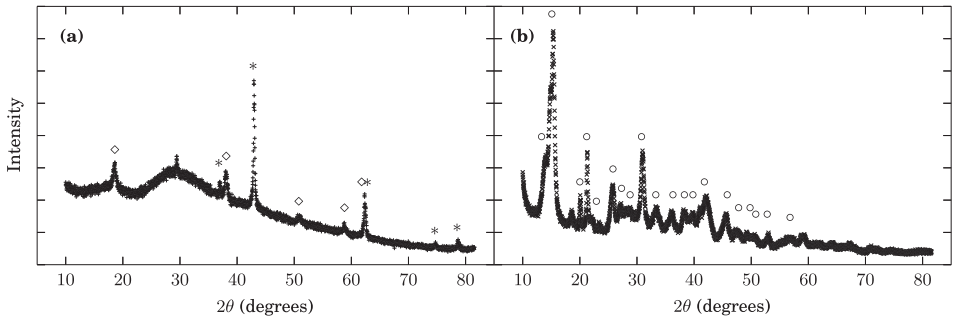

FIG. 2. XRD patterns measured after the neutron scattering experiments. (a) The diffraction peaks of DRY originate from the traces of unreacted MgO in the sample: the diamonds mark the peaks from brucite and asterisks the peaks from periclase phases. (b) The appearance of the hydromagnesite diffraction peaks (marked with circles) in U2 indicates partial crystallization of Upsalite during the experiment. The diffraction angle of 15° corresponds to a momentum transfer $q = 1$ Å^{-1} and 21° to $q = 1.5$ Å^{-1} in the neutron spectra.

similar systems (see the discussion in Section III A and, for example, Ref. 42), we expected this temperature range to be adequate to resolve the dynamics of water. However, post-experiment data analysis proved that an extended temperature range was needed. Therefore, U2 was measured for 6.25 h at 3 K and at 14 temperatures between 150 K and 360 K. The MCM-41 sample was cooled down to 140 K and subsequently the temperature was ramped to 290 K at a rate of 9.4 K/h. The acquired spectra were then averaged over 10 K temperature ranges except for the lowest and highest temperatures where the averages were over the ranges 140–175 K and 275–290 K. Finally, DRY was measured for 6.25 h at 3, 200, 300, and 360 K. All samples were weighed before and after the experiments to make sure that no leakage was present in the sample cells. During the U1 experiment, the instrument housing was filled with argon to reduce background from air scattering.

The raw neutron count data from SPHERES were binned and normalized to the accumulation time by instrument's standard data reduction program SLAW[43] yielding raw scattering spectra $N(q, \omega, T)$. After excluding data from the three lowest and one highest scattering angle detectors due to poor signal-to-noise ratios or unexpected increases in the background levels, our experiments covered the momentum transfer range 0.35 Å$^{-1} \le q \le 1.8$ Å^{-1} and the energy transfer range $-30.8\ \mu\text{eV} < \hbar\omega < 31.1\ \mu\text{eV}$. With the conversion factor $\hbar = 0.658\ \mu\text{eV} \cdot \text{ns}$, the resolution half width at half maximum of about 0.3 μeV, and the maximum energy transfer of about 30 μeV, we can estimate the order of magnitude of resolvable relaxation times as 10 ps–1 ns. The per spectrum signal-to-noise ratios ranged from 490 to 1450 for U1 and from 380 to 1200 for U2. The slightly worse values for U2 probably result from additional scattering from the air atmosphere in the instrument housing.

III. DATA ANALYSIS

A. Raw data inspection and comparison with MCM-41

Before discussing the data analysis and results of the QENS experiments in detail, it is worthwhile to take a look at the general features of the Upsalite spectra and compare them to the hydrated MCM-41 reference. The behavior of water in MCM-41 has been studied numerous times before[8,22–29] and thus it can be regarded as a well known model system. For this analysis, the U1, U2, and MCM-41 spectra were averaged over 0.60 Å$^{-1} \le q \le 1.7$ Å^{-1} and normalized to the corresponding maximum intensity at the lowest experimental temperature. No dry matrix or empty cell data were subtracted from the spectra as these corrections are not relevant for the following qualitative discussion.

Fig. 3 gives an overview of the spectral features of hydrated MCM-41, U1, and U2 as functions of temperature. The features of interest are the maximum height of the elastic peak I_{max} (Fig. 3(a)), the height of the quasielastic wings I_{wing} (intensity averaged over $-3\ \mu\text{eV} < \hbar\omega < -1\ \mu\text{eV}$, Fig. 3(b)), and the height of the background I_{bkg} (intensity averaged over $\hbar\omega < -25\ \mu$eV, Fig. 3(c)).

For MCM-41, Fig. 3 shows very clearly that there is one main relaxation process that moves with increasing temperature through the energy window of SPHERES: at low temperatures, the quasielastic scattering is unresolved and contributes to the resolution-broadened elastic line. With temperatures increasing towards 230 or 270 K, there is an increasing quasielastic intensity in the energy window $\hbar\omega = 1 \ldots 3\ \mu$eV or $25 \ldots 30\ \mu$eV. At even higher temperatures, the spectrum becomes so broad that the integral over the specific energy window decreases.

For Upsalite, the trend is basically the same, but less pronounced. The elastic peak decays much slower with increasing temperature, and the maxima in the quasielastic intensities are much weaker and are reached at much higher temperatures than in MCM-41. Compared to MCM-41, the dynamics of water appear to be strikingly slow in Upsalite. In MCM-41 it is difficult to resolve the dynamics above 250 K with the high-resolution spectrometer used here, as the quasielastic part of the spectra broadens to a nearly constant background. In Upsalite, on the other hand, there is a strong elastic component even above the melting point and the quasielastic wings remain discernible up to 360 K although the presence of a broad inelastic component is evident from I_{bkg}.

Data for the two samples U1 and U2 are in good accord. The constant difference in I_{bkg} can have a number of technical causes; the experiments were performed with more than one year interval, and for the U2 measurement, argon filling of the secondary spectrometer was not available. The other

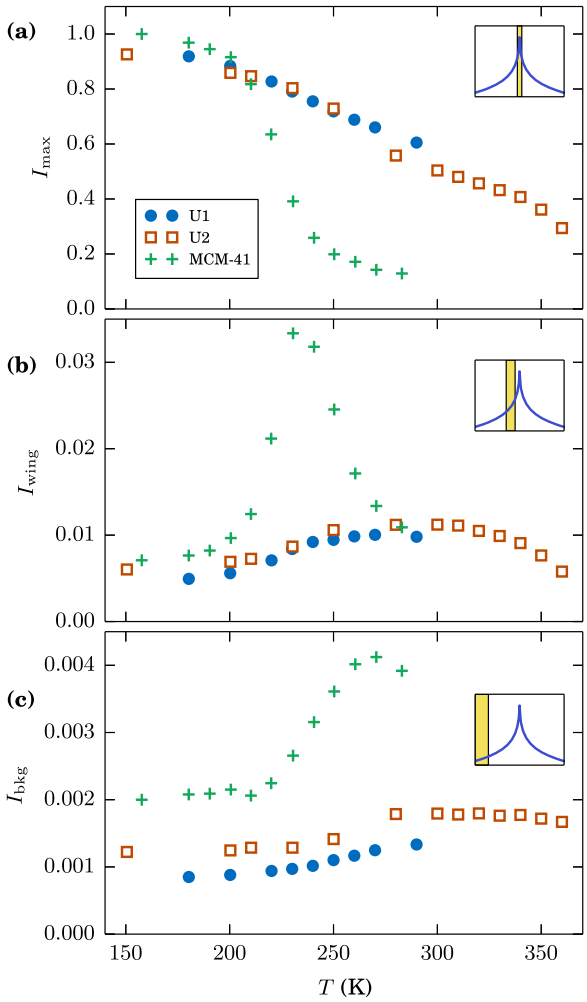

FIG. 3. Evolution of spectral features of water confined in different materials for spectra averaged over 0.60 Å^{-1} $\leq q \leq$ 1.7 Å^{-1}: MCM-41 (porous silica, crosses), U1 (filled circles), and U2 (empty squares). (a) Maximum of the elastic line. (b) Average height of the elastic wing $-3\,\mu\text{eV} < \hbar\omega < -1\,\mu\text{eV}$. (c) Average height of the background $\hbar\omega < -25\,\mu\text{eV}$. In the insets, the areas shaded in yellow show schematically which part of the spectra the plotted data represent.

noticeable difference is the apparent jump of $I_{max}(T)$ for U2 between 250 and 280 K (Fig. 3(a)), likely due to melting of the frozen water fraction.

B. Further data reduction

Instrument resolution functions $R(q,\omega)$ for U1 and U2 were obtained from the corresponding raw spectra $N(q,\omega,3\,\text{K})$ by subtracting linear backgrounds $B^{\text{raw}}(q,\omega)$ and normalizing with respect to the integrals over the experimental ω range,

$$R(q,\omega) = \frac{N(q,\omega,3\,\text{K}) - B^{\text{raw}}(q,\omega)}{\int_{-\omega_\text{l}}^{\omega_\text{l}} \text{d}\omega \left[N(q,\omega,3\,\text{K}) - B^{\text{raw}}(q,\omega)\right]}, \quad (1)$$

where $\hbar\omega_\text{l} = 30.5\,\mu\text{eV}$. The backgrounds were fitted to the low ($\hbar\omega < -20\,\mu\text{eV}$) and high ($\hbar\omega > 20\,\mu\text{eV}$) energy transfer tails of the raw 3 K spectra. To make the data from the two experiments comparable, the raw U1 and U2 spectra were normalized to vanadium references N_V,

$$I(q,\omega,T) = \frac{N(q,\omega,T)}{\int_{-\omega_\text{l}}^{\omega_\text{l}} \text{d}\omega \left[N_\text{V}(q,\omega) - B_\text{V}^{\text{raw}}(q,\omega)\right]}, \quad (2)$$

where the vanadium backgrounds B_V^{raw} were calculated similarly to B^{raw}. The background subtracted DRY data were normalized to vanadium as well,

$$D(q,\omega,T) = \frac{N_\text{DRY}(q,\omega,T) - B_\text{DRY}^{\text{raw}}(q,\omega)}{\int_{-\omega_\text{l}}^{\omega_\text{l}} \text{d}\omega \left[N_\text{V}(q,\omega) - B_\text{V}^{\text{raw}}(q,\omega)\right]}. \quad (3)$$

Due to instrument geometry effects,[44] small shifts in the elastic peak position are observable in SPHERES. In order to account for them, the DRY spectra were further shifted in ω so that the elastic peak maxima corresponded to the maxima in the resolution functions.

The shapes of the DRY spectra were not completely temperature independent (see Fig. S1 in the supplementary material). The total scattering intensity decreased when the temperature was raised from 3 to 360 K. Also, a slight broadening of the elastic peak was observed. Therefore it was not sufficient to use $D(q,\omega)$ measured at a single temperature as the matrix contribution for all the hydrated spectra. Instead, a linearly weighted sum was used to interpolate the DRY spectra to the intermediate temperatures corresponding to what was used for U1 and U2,

$$D^{\text{interp}}(q,\omega,T) = \frac{T_\text{high} - T}{T_\text{high} - T_\text{low}} D(q,\omega,T_\text{low}) + \frac{T - T_\text{low}}{T_\text{high} - T_\text{low}} D(q,\omega,T_\text{high}), \quad (4)$$

where T is the temperature to which to interpolate while T_low is the temperature below and T_high the temperature above T of the measured DRY spectra.

For plotting purposes only, the spectra were smoothed by convolution with a von Hann ("Hanning") window.[45] The error bars in the fit parameter plots are estimated errors with regards to the experimental uncertainties and were calculated from the variance-covariance matrix of the free fitting parameters.

C. Development of the physical model

A general model describing the experimental spectra $I(q,\omega,T)$ is given by

$$S(q,\omega,T) = f_\text{water}(q,T) S_\text{water}(q,\omega,T) \otimes R(q,\omega) + f_\text{DRY} D(q,\omega,T) + B(q,\omega). \quad (5)$$

The physical model for the dynamics of water molecules is contained within S_water which will be later defined such that its integral over all ω is 1. Therefore, to relate S_water to the experimental spectra, it has to be scaled by the total scattering intensity from water,

$$f_\text{water}(q,T) = \int_{-\omega_\text{l}}^{\omega_\text{l}} \text{d}\omega \left[I(q,\omega,T) - B(q,\omega)\right] - f_\text{DRY} \int_{-\omega_\text{l}}^{\omega_\text{l}} \text{d}\omega D(q,\omega,T). \quad (6)$$

Subsequently, S_{water} is convoluted with the instrumental resolution R. We chose to include the scattering from the matrix and sample cell D (or D^{interp}) to the fit function since subtracting this contribution directly from the experimental spectra leads to increased statistical uncertainties. D in turn is weighted by f_{DRY}, the ratio of the masses of Upsalite between the hydrated and the DRY samples. In the case of U1, $f_{\text{DRY}} = 1.388$ g/g while for U2, $f_{\text{DRY}} = 1.219$ g/g. The linear backgrounds $B(q, \omega)$ were obtained from the normalized U1 and U2 spectra $I(q, \omega, 3\,\text{K})$, similarly to the raw backgrounds.

As discussed in Section III A, the limited energy window of the spectrometer will break the treatment of the total relaxation into three distinct regimes. This will be reflected in how S_{water} will be constructed in the following.

Slow relaxation processes out of the dynamical window of a neutron spectrometer will appear as an elastic line. According to the discussion in Section III A, such dynamically frozen states persist in U1 and U2 over the entire temperature range. This prompts us to write S_{water} as a weighted sum of a delta function $\delta(\omega)$ and a fit function $M(q, \omega, T)$ describing the resolvable dynamics,

$$S_{\text{water}}(q, \omega, T) = a(q, T)\delta(\omega) + [1 - a(q, T)]\, M(q, \omega, T), \quad (7)$$

where the relative weights of the two contributions are denoted by the elastic fraction a.

Heterogeneous relaxation times are expected in confined water systems due to the high surface-to-volume ratio of the confining matrix. The stretched exponential function $\exp[(t/\tau)^{\beta}]$ describes this type of dynamics without introducing an unmanageable amount of free parameters. When operating in the ω space instead of t, a Fourier transform has to be applied to the relaxation function, and in the case of the stretched exponential, the result is known as the Kohlrausch-Williams-Watts (KWW) function. Fitting the data at hand using the KWW as M resulted, however, in a stretch exponent β close to 1 for all temperatures and q values. Thus we fixed $\beta = 1$ for all fits effectively reducing the KWW to a Cauchy-Lorentz function.

Since the Lorentzian may have a sharp peak, the convolution with the resolution in (5), when computed discretely, may result in large errors.[46] To circumvent the problem, we averaged the function over each energy bin giving

$$M(\omega_i, \tau) = \frac{1}{\Delta\omega} \int_{\omega_i - \Delta\omega/2}^{\omega_i + \Delta\omega/2} \mathrm{d}\omega \frac{\tau}{\pi \left[1 + (\omega\tau)^2\right]}, \quad (8)$$

where $\Delta\omega$ is the bin width, ω_i the center of the ith bin, and τ the relaxation time.

Fitting with (5)–(8) and with free τ raised two issues. The first was the degeneracy between the elastic line and the Lorentzian at long relaxation times.[42] Slow relaxations indicate a sharply peaked model function which in turn becomes indistinguishable from the delta function in (7). The delta function, however, cannot be accounted for by the Lorentzian alone: setting $a = 0$ did not result in acceptable fits. The degeneracy is relevant especially at low temperatures and at low q. To make fitting stable and reproducible, we decided to remove the q dependences from τ. In the case of τ, the q dependence is relatively weak at high q, thus allowing for a q independent approximation. At low q, on the other hand, the assumption of q independent τ breaks down. However, due to the degeneracy of the Lorentzian and the delta functions, fitting with (5)–(8) is still possible as the sharp peak of the Lorentzian caused by high τ "escapes" to the delta function. Consequently, we expect τ extracted from the fits to give a rough estimate for the relaxation times at high q while at low q and low temperatures, τ represents a lower limit for the relaxation time. In this case, the extracted a indicates an upper limit for the fraction of immobile water in the sample.

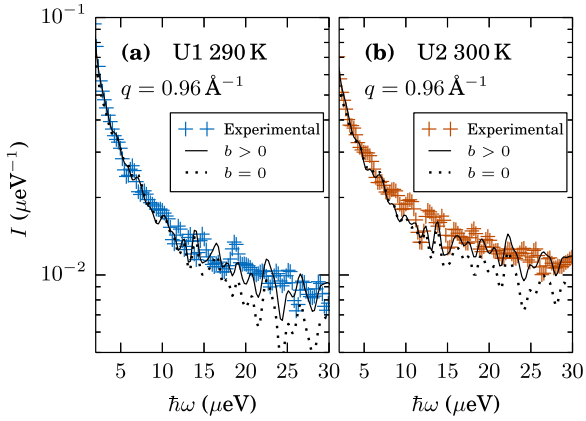

FIG. 4. The extreme tails of the normalized spectra (crosses) at $q = 0.96$ Å^{-1}: (a) U1 at 290 K; (b) U2 at 300 K. The lines are fits to (5)–(9). The fit shown by the continuous line has a finite additional constant background b while for the dotted line, $b = 0$. The oscillation-like features at the high $\hbar\omega$ tails of the fits result from the noise in the experimental instrument resolution and DRY spectrum included in the fits.

The second issue was the systematic deviation of the fits from the experimental spectra at the extreme energy transfer tails. Even though a part of it may result from the genuine temperature dependent background of the instrument, a comparison to the background levels of the DRY spectra showed that the hydrated samples contain an additional broad inelastic intensity arising from fast out-of-window dynamics, as discussed in Section III A. These are mostly flat in the energy window of the spectrometer and thus can be modeled as an additional constant background b,

$$\tilde{S}(q, \omega, T) = S(q, \omega, T) + b(q, T). \quad (9)$$

The difference between fits with and without b is exemplified in Fig. 4.

In the end, we were left with three fitting parameters: the elastic fraction a and background from a broad inelastic component b which qualitatively describe how the distribution of relaxation times behaves as a function of temperature with regards to the energy transfer window of the spectrometer, and the relaxation time τ.

IV. RESULTS: DYNAMICS OF CONFINED WATER

Representative spectra at selected temperatures from U1 and U2 as well as fits to (5)–(9) at $q = 0.96$ Å^{-1} are shown in

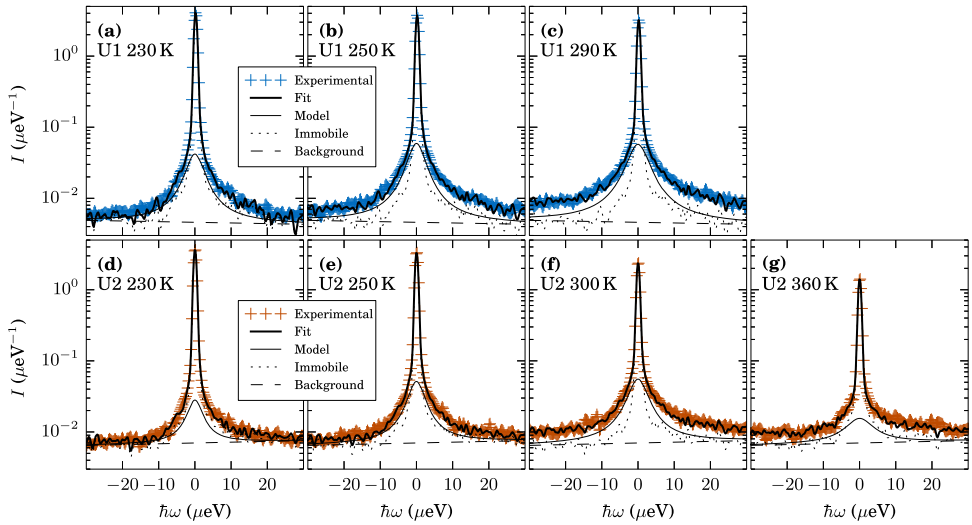

FIG. 5. Normalized experimental spectra of hydrated Upsalite at $q = 0.96$ Å^{-1} (crosses): (a) U1 at 230 K, (b) U1 at 250 K, (c) U1 290 K, (d) U2 at 230 K, (e) U2 at 250 K, (f) U2 at 300 K, and (g) U2 at 360 K. The thick solid lines are fits with (5)–(9). Also shown are the contribution from the scaled Lorentzian function $(1-a)f_{\text{water}}M(q,\omega,T)+B$ (thin solid lines) and the total contribution from immobile water, Upsalite matrix and sample cell $af_{\text{water}}R(q,\omega)+f_{\text{DRY}}D(q,\omega,T)+B$ (dotted lines). The instrument backgrounds B are shown as dashed lines.

Fig. 5 (for the rest of the spectra, see supplementary material). By visual inspection, the fits are of acceptable quality throughout the T and q ranges. The development of the quasielastic wings due to mobile water molecules can be observed by comparing the experimental spectra with the immobile contribution (immobile water, Upsalite matrix, and sample cell; dotted lines in the figure). At 230 K (Figs. 5(a) and 5(d)), the wings are relatively weak. Nevertheless, their presence confirms the existence of liquid phase in the samples. At higher temperatures, the wings become more pronounced as the mobility of water molecules increases. The Lorentzian model function (8), also plotted in Fig. 5, becomes more pronounced between 230 K and 250 K as a larger portion of mobile water molecules enters spectrometer's energy transfer window. Also, an additional background component appears to the spectra which is a sign of out-of-window fast dynamics. At 360 K (Fig. 5(g)), the model function flattens implying that an increasing amount of fast dynamical states outside the spectrometer window become occupied.

A. Fast out-of-window dynamics

Dynamics too fast for a high-resolution spectrometer such as SPHERES will cause neutrons to "leak" out of the energy transfer window which effectively decreases the observed total scattering intensity from water, f_{water}, defined in (6). These neutrons contribute to the broad inelastic background b or to even higher energy modes such as phonons escaping detection completely. As shown in Fig. 6, f_{water} decreases with increasing temperature which, conversely, indicates an increasing amount of out-of-window scattering. This is expected, as higher temperatures enable the occupancy of faster dynamical states.

Most of the out-of-window scattering contributes to the broad inelastic component increasing b as depicted in Fig. 7. Basically, three q dependent regimes are observed: At low q, b increases significantly only for $T > 330$ K. When

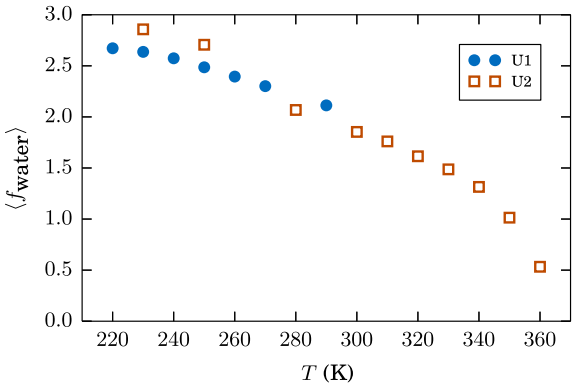

FIG. 6. The total scattering intensities from water f_{water} [see Equation (6)] averaged over the experimental q range for U1 (filled circles) and U2 (empty squares) as functions of temperature.

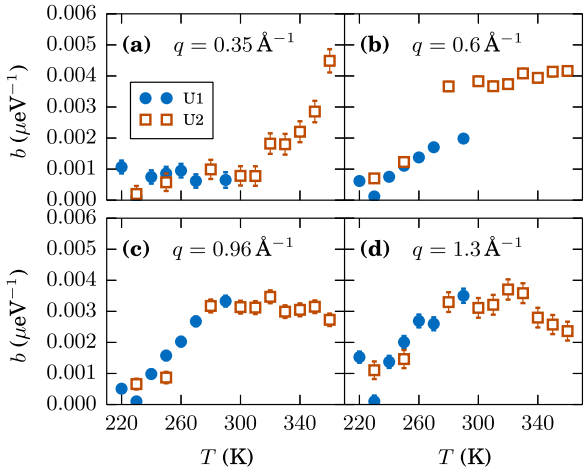

FIG. 7. The additional background term b as a function of temperature for U1 (filled circles) and U2 (empty squares) at (a) $q = 0.35$ Å^{-1}, (b) $q = 0.60$ Å^{-1}, (c) $q = 0.96$ Å^{-1}, and (d) $q = 1.3$ Å^{-1}.

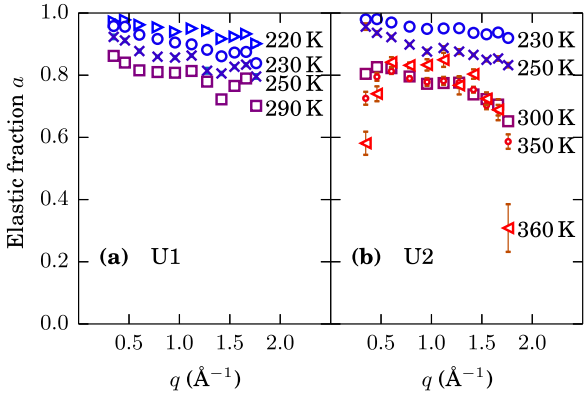

FIG. 8. Fraction of elastic scattering a from immobile water as a function of q in (a) U1 and (b) U2.

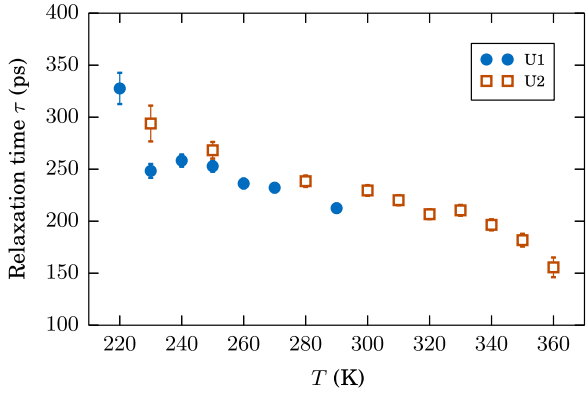

FIG. 10. The fitted relaxation times τ of the Lorentzian model function (8) as functions of temperature for U1 (filled circles) and U2 (empty squares).

$q \geq 0.60$ Å^{-1}, b saturates above 280 K. Additionally, b further starts to decrease above $q = 0.96$ Å^{-1}, above 330 K indicating further broadening of the component.

B. Dynamically frozen water

A substantial amount of water is seen as dynamically frozen by the spectrometer even at the highest temperatures. This is evident from the high fractions of elastic scattering shown in Fig. 8. With the exception of U2 at 360 K, a stays above ~0.6 indicating that only a minority of the water molecules contribute to the in-window quasielastic signal.

For U2, the values of a decrease as temperature is increased up to around 300 K. In spite of the step noticed in Fig. 3, melting does not seem drastically affecting the parameter. Between 300 and 340 K, a stays roughly at the same values over the whole q range. However, f_{water} decreases at the same time (Fig. 6), so only the ratio between elastic and quasielastic scattering remains unchanged and the total amount of dynamically frozen water actually decreases. Above 340 K, a increases in the mid-q range while decreasing at low and high q. This high temperature mid-q behavior is linked to partial matrix crystallization at the last stages of the experiment. As anticipated in Sec. II B, we conclude that no significant crystallization took place before 330 K was reached during the U2 experiment. That being said, the reaction between water and Upsalite would lead to hydrogen atoms being trapped into the hydromagnesite or nesquehonite phases as chemically bound species or as a part of water of crystallization. Assuming that all elastic scattering originates from hydrogens in the crystalline phase at 360 K, we get $f_{\text{water}}(360\,\text{K})/f_{\text{water}}(3\,\text{K}) \cdot \max[a(360\,\text{K})] = 0.18$, that is, up to 18% of hydrogens would be embedded in the crystalline phase at the end of the experiment.

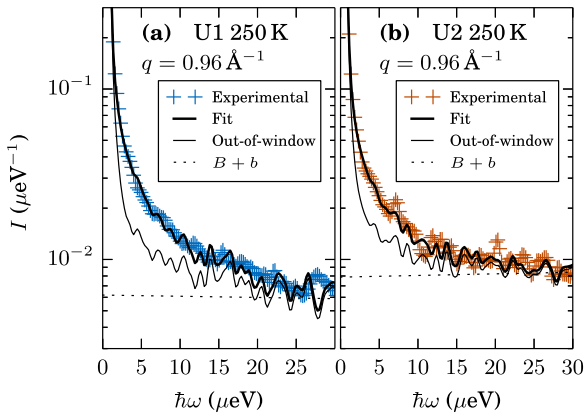

FIG. 9. Comparison of the experimental spectra from hydrated Upsalite (crosses) with contributions out of spectrometer's energy transfer window (dotted lines) in the quasielastic $\hbar\omega$ region for (a) U1 and (b) U2. The out-of-window contributions consist of the instrument resolution broadened elastic line and broad inelastic component and are calculated by subtracting the in-window contribution from (9): $\tilde{S} - f_{\text{water}} S_{\text{water}} \otimes R$.

C. In-window dynamics

Fig. 9 exemplifies the contribution of dynamics in the energy transfer window of the spectrometer to the total experimental spectra. Shown in the figure is a comparison between the experimental spectra and fits to (5)–(9), with the in-window contribution $f_{\text{water}} S_{\text{water}} \otimes R$ subtracted. This leaves contributions from the resolution broadened elastic line and from the broad inelastic component. The difference in the curves close to the elastic peak is due to the quasielastic in-window scattering and suggests a quantifiable contribution even for U2 in spite of the slightly worse signal-to-noise ratio.

The in-window dynamics of water are quantified by the relaxation time τ extracted from the fits with (5)–(9). The results are gathered in Fig. 10. Below 240 K, the elastic fraction a reaches values close to 1 rendering fitting difficult, and consequently, there are increased uncertainties in τ. Nevertheless, the relaxation time stays at unexpectedly high level even above the room temperature. This is due to the limited dynamical window of the spectrometer, as discussed in Section V. Data from both U1 and U2 match each other reasonably well, considering the differences in the hydration levels.

V. DISCUSSION

The dynamics of water confined in hydrated Upsalite can be divided into three classes with regards to spectrometer's energy transfer window: First, dynamically frozen water which is seen as an elastic delta line is quantified by the elastic fraction a. This includes also water in the ice phase up to the melting point. Second, the in-window dynamics result in a quasielastic line, width of which is proportional to $1/\tau$. Third, the broad

inelastic background which stems from the fast dynamics gives rise to the additional background term b.

These different regimes can be identified in both U1 and U2 with regards to temperature and q. Below 200 K, water is dynamically frozen and only elastic scattering is observed. Above 200 K, the elastic line intensity starts to decrease and the quasielastic wings become discernible when dynamics of the coexisting liquid phase enter spectrometer's window. At temperatures above 230 K, an additional background appears at $q > 0.60$ Å^{-1} from a broad inelastic line resulting from fast local dynamics. Melting does not cause an appreciable decrease in the amount of dynamically frozen water. It seems that mobility remains rather low for the majority of the water molecules. Around 300 K, the in-window dynamics of U2 enter a state where there are no notable changes in τ; however, the decrease of total elastic and in-window scattering from water f_{water} indicates an increasing fraction of fast dynamical processes with increasing temperature. This persists up to 340 K, after which τ starts to decrease again. Also, at low and high ends of the q range, the elastic line intensity decreases together with the appearance of the broad inelastic line at $q \leq 0.60$ Å^{-1} and considerable broadening of the line at $q \geq 1.3$ Å^{-1} as indicated by the decrease in b. This may be due to an increased fraction of water molecules being in the gas phase, e.g., as moisture in the air between the Upsalite grains. A rough calculation based on the partial pressure of water vapor in a closed system shows that 42% of water molecules are in the gas phase at 90 °C (363 K). This would enable long range displacements increasing b at low q while considerably broadening the inelastic background at high q as local dynamical states such as rotational motions became increasingly populated.

Over the experimental temperature range, τ reaches values between 150 and 350 ps, with rather weak temperature dependence as Fig. 10 shows. This deviates from the usual behavior of both bulk and confined water, where the relaxation time is found to follow a stronger temperature dependence than the Arrhenius law $\tau \propto \exp[-E_{\mathrm{A}}/(k_{\mathrm{b}}T)]$ (E_{A} is the activation energy and k_{b} the Boltzmann constant).[47] At all temperatures, there is a strong elastic line present. Additionally, fast dynamics contribute to an observable broad inelastic line except for low temperatures. The coincident presence of slow and fast out-of-window components indicates that the spread of relaxation times is broader than what is accessible with the SPHERES spectrometer. Therefore, except for the few lowest temperatures, τ takes nearly constant values characteristic to the $\hbar\omega$ window. In these cases, τ cannot be used to quantify the relaxation processes. On the other hand, when no broad component is present at the lowest temperatures, τ does give a lower limit for the relaxation time.

The most notable feature of water confined in Upsalite is the persistence of slow relaxations up to the highest experimental temperature. As Fig. 8 shows, there is a strong elastic line in U2 even at 360 K. For comparison, the residence time for bulk water at room temperature is about 2 ps,[48] which would produce only the broad inelastic component in the energy transfer window of the SPHERES spectrometer. This is also in stark contrast with MCM-41 and water confined in carbon nanohorns[42] in which the quasielastic part of the spectra quickly broadened to an almost constant background well below the freezing point. One would expect such slow processes as in Upsalite to be found in interfacial water bound to a hydrophilic surface.[20,34,49,50]

A recent dielectric spectroscopy study on calcinated Upsalite at room temperature and at 95% relative humidity (hydration level ≈ 0.22 g/g) revealed that, according to the static permittivity of the hydrated sample, a fraction of ~0.5 of water could be classified as bound.[51] This corresponds to 0.11 g of bound water per 1 g of Upsalite. Assuming the same bound water content in U1 would mean a fraction of 0.11/0.367 = 30% of bound water while, in the case of U2, the fraction would be 0.11/0.463 = 24%. The existence of such bound water would explain the amount of dynamically frozen water in U1 and U2 above the freezing point and that melting does not produce strong changes in system's parameters. The lack of quantifiable q dependency in τ at low temperatures also indicates a non-diffusive origin for the observed dynamics.

VI. SUMMARY AND CONCLUSIONS

In the present analysis of water confined in the pores of Upsalite, we find surprisingly slow relaxation times even above the melting point of water. A strong elastic line from dynamically frozen water persists over the experimental temperature range up to 360 K, while at the same time, in-window quasielastic scattering remains resolvable even with the high-resolution neutron spectrometer used for this study. These findings deviate considerably from the well-established behavior of confined water in many other systems. Ordinarily, the dynamics become too fast to track with similar spectrometers already below the freezing point as is the case with MCM-41 discussed in Section III or water in carbon nanohorns.[42] The high temperature slow dynamics of water confined in Upsalite seem to originate from interfacial-like bound water whose amount is considerably higher than in comparable systems, especially considering that the supposedly hydrophilic organic residues at the pore walls of as-synthesized Upsalite have been removed. Even though partial crystallization of the Upsalite matrix in U2 occurred during the two or three last temperature steps of the experiment, the results up to 330 K should not be considerably disturbed by hydrogens bound to the nesquehonite or hydromagnesite phases.

SUPPLEMENTARY MATERIAL

See supplementary material for DRY spectra, details of U1, U2, and MCM-41 sample preparation and experiments, as well as for the complete set of U1 and U2 spectra and fits.

ACKNOWLEDGMENTS

The authors from Uppsala University wish to thank the Swedish Research Council and Vinnova for financial support.

[1] M. A. Ricci, F. Bruni, and A. Giuliani, Faraday Discuss. **141**, 347 (2009).
[2] F. G. Alabarse, J. Haines, O. Cambon, C. Levelut, D. Bourgogne, A. Haidoux, D. Granier, and B. Coasne, Phys. Rev. Lett. **109**, 035701 (2012).

[3]A. I. Kolesnikov, J.-M. Zanotti, C.-K. Loong, P. Thiyagarajan, A. P. Moravsky, R. O. Loutfy, and C. J. Burnham, Phys. Rev. Lett. **93**, 035503 (2004).
[4]O. Byl, J.-C. Liu, Y. Wang, W.-L. Yim, J. K. Johnson, and J. T. Yates, J. Am. Chem. Soc. **128**, 12090 (2006).
[5]M. Rovere, M. A. Ricci, D. Vellati, and F. Bruni, J. Chem. Phys. **108**, 9859 (1998).
[6]S. Takahara, S. Kittaka, T. Mori, Y. Kuroda, T. Yamaguchi, and M.-C. Bellissent-Funel, Adsorption **11**, 479 (2005).
[7]P. Gallo, M. Rovere, and S.-H. Chen, J. Phys.: Condens. Matter **22**, 284102 (2010).
[8]C. E. Bertrand, K.-H. Liu, E. Mamontov, and S.-H. Chen, Phys. Rev. E **87**, 042312 (2013).
[9]M. F. Harrach, F. Klameth, B. Drossel, and M. Vogel, J. Chem. Phys. **142**, 034703 (2015).
[10]S. H. Lee and P. J. Rossky, J. Chem. Phys. **100**, 3334 (1994).
[11]J. Jelassi, T. Grosz, I. Bako, M.-C. Bellissent-Funel, J. C. Dore, H. L. Castricum, and R. Sridi-Dorbez, J. Chem. Phys. **134**, 064509 (2011).
[12]D. E. Rosenfeld and C. A. Schmuttenmaer, J. Phys. Chem. B **115**, 1021 (2011).
[13]J. Forsgren, S. Frykstrand, K. Grandfield, A. Mihranyan, and M. Strømme, PLoS One **8**, e68486 (2013).
[14]P. Zhang, J. Forsgren, and M. Strømme, Int. J. Pharm. **472**, 185 (2014).
[15]P. Zhang, T. Zardán Gómez de la Torre, J. Forsgren, C. A. Bergström, and M. Strømme, J. Pharm. Sci. **105**, 657 (2016).
[16]S. Frykstrand, J. Forsgren, P. Zhang, M. Strømme, and N. Ferraz, J. Biomater. Nanobiotechnol. **6**, 257 (2015).
[17]S. Frykstrand, J. Forsgren, O. Cheung, P. Zhang, J. Hong, M. Strømme, and N. Ferraz, RSC Adv. **6**, 52810 (2016).
[18]M.-C. Bellissent-Funel, K. Bradley, S. Chen, J. Lal, and J. Teixeira, Physica A **201**, 277 (1993).
[19]M.-C. Bellissent-Funel, S. H. Chen, and J.-M. Zanotti, Phys. Rev. E **51**, 4558 (1995).
[20]J.-M. Zanotti, M.-C. Bellissent-Funel, and S.-H. Chen, Phys. Rev. E **59**, 3084 (1999).
[21]M. C. Bellissent-Funel, S. Longeville, J. M. Zanotti, and S. H. Chen, Phys. Rev. Lett. **85**, 3644 (2000).
[22]S. Takahara, M. Nakano, S. Kittaka, Y. Kuroda, T. Mori, H. Hamano, and T. Yamaguchi, J. Phys. Chem. B **103**, 5814 (1999).
[23]F. Mansour, R. M. Dimeo, and H. Peemoeller, Phys. Rev. E **66**, 041307 (2002).
[24]A. Faraone, L. Liu, C.-Y. Mou, P.-C. Shih, J. R. D. Copley, and S.-H. Chen, J. Chem. Phys. **119**, 3963 (2003).
[25]S. Takahara, N. Sumiyama, S. Kittaka, T. Yamaguchi, and M.-C. Bellissent-Funel, J. Phys. Chem. B **109**, 11231 (2005).
[26]F. Mallamace, M. Broccio, C. Corsaro, A. Faraone, L. Liu, C.-Y. Mou, and S.-H. Chen, J. Phys.: Condens. Matter **18**, S2285 (2006).
[27]J. Sjöström, J. Swenson, R. Bergman, and S. Kittaka, J. Chem. Phys. **128**, 154503 (2008).
[28]D. W. Hwang, C. C. Chu, A. K. Sinha, and L. P. Hwang, J. Chem. Phys. **126**, 044702 (2007).
[29]M. Sattig, S. Reutter, F. Fujara, M. Werner, G. Buntkowsky, and M. Vogel, Phys. Chem. Chem. Phys. **16**, 19229 (2014).
[30]A. Schreiber, I. Ketelsen, and G. H. Findenegg, Phys. Chem. Chem. Phys. **3**, 1185 (2001).
[31]S. Jähnert, F. Vaca Chávez, G. E. Schaumann, A. Schreiber, M. Schönhoff, and G. H. Findenegg, Phys. Chem. Chem. Phys. **10**, 6039 (2008).
[32]E. Mamontov, J. Chem. Phys. **121**, 9087 (2004).
[33]J. Swenson, H. Jansson, W. S. Howells, and S. Longeville, J. Chem. Phys. **122**, 084505 (2005).
[34]E. Mamontov, L. Vlcek, D. J. Wesolowski, P. T. Cummings, W. Wang, L. M. Anovitz, J. Rosenqvist, C. M. Brown, and V. Garcia Sakai, J. Phys. Chem. C **111**, 4328 (2007).
[35]S. Frykstrand, J. Forsgren, A. Mihranyan, and M. Strømme, Microporous Mesoporous Mater. **190**, 99 (2014).
[36]M. Grün, I. Lauer, and K. K. Unger, Adv. Mater. **9**, 254 (1997).
[37]G. H. Findenegg, S. Jähnert, D. Akcakayiran, and A. Schreiber, ChemPhysChem **9**, 2651 (2008).
[38]S. Kittaka, S. Ishimaru, M. Kuranishi, T. Matsuda, and T. Yamaguchi, Phys. Chem. Chem. Phys. **8**, 3223 (2006).
[39]M. C. Bellissent-Funel, J. Lal, and L. Bosio, J. Chem. Phys. **98**, 4246 (1993).
[40]J. Wuttke, A. Budwig, M. Drochner, H. Kämmerling, F.-J. Kayser, H. Kleines, V. Ossovyi, L. C. Pardo, M. Prager, D. Richter, G. J. Schneider, H. Schneider, and S. Staringer, Rev. Sci. Instrum. **83**, 075109 (2012).
[41]H. Maier-Leibnitz Zentrum, J. Large-Scale Res. Facil. **1**, A30 (2015).
[42]M.-C. Bellissent-Funel, K. Kaneko, T. Ohba, M.-S. Appavou, A. J. Soininen, and J. Wuttke, Phys. Rev. E **93**, 022104 (2016).
[43]J. Wuttke, SLAW: neutron histogram to scattering law converter http://apps.jcns.fz-juelich.de/man/slaw.html.
[44]J. Wuttke and M. Zamponi, Rev. Sci. Instrum. **84**, 115108 (2013).
[45]See http://scipy-cookbook.readthedocs.org/items/SignalSmooth.html for a signal smoothing algorithm written in Python.
[46]J. Wuttke, Algorithms **5**, 604 (2012).
[47]J. Teixeira, M.-C. Bellissent-Funel, S. H. Chen, and A. J. Dianoux, Phys. Rev. A **31**, 1913 (1985).
[48]J. J. Tuck, P. L. Hall, M. H. B. Hayes, D. K. Ross, and C. Poinsignon, J. Chem. Soc., Faraday Trans. 1 **80**, 309 (1984).
[49]J.-C. Perrin, S. Lyonnard, and F. Volino, J. Phys. Chem. C **111**, 3393 (2007).
[50]K. Yoshida, T. Yamaguchi, S. Kittaka, M.-C. Bellissent-Funel, and P. Fouquet, J. Phys.: Condens. Matter **24**, 064101 (2012).
[51]I. Pochard, S. Frykstrand, J. Eriksson, S. Gustafsson, K. Welch, and M. Strømme, J. Phys. Chem. C **119**, 15680 (2015).